JOURNAL OF THEORETICAL AND APPLIED MECHANICS
47, 2, pp. 435-456, Warsaw 2009

STABILITY AND LOAD CARRYING CAPACITY OF MULTI-CELL THIN-WALLED COLUMNS OF RECTANGULAR CROSS-SECTIONS

Marian Królak
Katarzyna Kowal-Michalska
Radosław J. Mania
Jacek Świniarski

Technical University of Lodz, Department of Strength of Materials and Structures, Łódź, Poland
e-mail: Marian.Krolak@p.lodz.pl

The paper concerns theoretical, numerical and experimental analysis of the stability and ultimate load of multi-cell thin-walled columns of rectangular and square cross-sections subjected to axial compression (uniform shortening of the column). The theoretical analysis deals with the local and global stability of multi-cell orthotropic columns of a rectangular profile with rectangular cells. It has been shown that for a multi-cell column made of the same material and having the same cross-section area, the value of local buckling stress of the column walls grows rapidly with an increase of the cell number. The experiment conducted for isotropic columns has also proved a significant growth of the ultimate load with the increase of the cell number. The paper gives some conclusions which can be useful in design of thin-walled box columns.

Key words: stability, ultimate load, thin-walled, multi-cell column

1. Introduction

Thin-walled columns and beams of flat walls are built of long rectangular plates connected on longitudinal edges. Compressed walls of such structures with a small thickness-to-width ratio ($t/b < 1/200$) undergo local buckling with small critical stress, comparing to the yield limit. To increase the local buckling load of these structures, longitudinal ribs are added whose stiffness is properly chosen (Maquoi and Massonet, 1971; Massonet and Maquoi, 1973). Parallel to the acting load, the ribs divide the column wall into a few plate-like

stripes. Their width is smaller than the plate itself. This causes a several times or even greater growth of the local buckling load when the cross section area increases not much.

In the present paper it has been suggested to increase the local buckling strength of a thin-walled single cell compressed column or a bent beam (box, girder) by substituting them with multi-cell structures. In the paper, the multi-cell structures of equal cross-section area, equal dimensions and made of the same material as a single cell structure will be considered to easily prove the increase of local buckling resistance for the first ones. In the world literature, there are surprisingly few works (Chen and Wierzbicki, 2001; Kim, 2002) dealing with the problems of stability, post-buckling behaviour and ultimate stress of prismatic beam-columns of multi-cell cross-sections.

2. Local buckling analysis of thin-walled orthotropic columns with a rectangular cross-section under edgewise compression

Let us consider a long prismatic multi-cell column subjected to compression with a cross-section shown in Fig. 1b, and a single cell column (box column) presented in Fig. 1a.

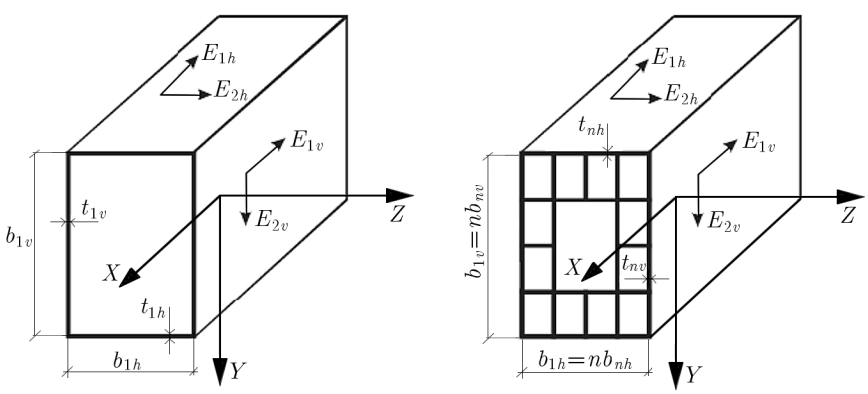

Fig. 1. Considered cross-sections of analysed columns

The following notation will be introduced:

- n – number of cells adjacent to one wall
- b_{1v}, b_{1h} – height/width of column cross-section
- t_{1v}, t_{1h} – thickness of vertical/horizontal walls of single cell column

b_{nv}, b_{nh} – height/width of cell
t_{nv}, t_{nh} – thickness of vertical/horizontal walls of multi-cell column
L – length of column.

In further considerations we assume that:
all walls are made of an orthotropic material of elastic constants E_1, E_2, G, ν_{12}, ν_{21}
E_1 – elastic modulus in the longitudinal direction (direction of compression)
E_2 – elastic modulus in the direction perpendicular to the column axis
G – Kirchhoff's modulus
ν_{12}, ν_{21} – Poisson's ratios.

In order to compare the values of local buckling stress for single-cell and multi-cell columns it is assumed that the overall dimensions of the cross-section areas of the analysed columns are the same. In this work, the geometric and material parameters of thin-walled single and multi-cell columns are chosen in such a way that the local buckling of all walls occurs at the same value of compressive loading. In such a case, all walls can be treated as simply supported along all edges.

In further considerations it is assumed that the column overall dimensions provide the global stability of the structure. It is assumed too, that the local-global buckling interaction does not occur. In paper Królak and Kowal-Michalska (2004b) detailed theoretical analysis of global and local buckling of thin-walled multi-cell rectangular profiles (particularly square) made of an orthotropic material is described. For columns which fulfill the above assumptions given in Królak and Kowal-Michalska (2004b), Volmir (1968), the following approximate relations were obtained:

- For single-cell column buckling stress

$$\sigma_{cr1}^{loc} = k\frac{\pi^2 E_1}{12\gamma}\Big(\frac{t_{1h}}{b_{1h}}\Big)^2 = k\frac{\pi^2 E_1}{12\gamma}\Big(\frac{t_{1v}}{b_{1v}}\Big)^2 \tag{2.1}$$

where k is the buckling load factor, which for long plates simply supported along all edges is taken as $k = 4$, γ – coefficient which depends on elastic constants; its inverse has the form

$$\frac{1}{\gamma} = \frac{\frac{1}{2}\sqrt{\frac{E_1}{E_2}} + \frac{1}{2}\frac{E_2\nu_{12}}{E_1} + \frac{G}{E_1}\Big(1 - \frac{E_2\nu_{12}^2}{E_1}\Big)}{1 - \frac{E_2\nu_{12}^2}{E_1}} \tag{2.2}$$

where the elasticity constants fulfill Betty's relation $\nu_{12}E_1 = \nu_{21}E_2$.

Formulas (2.1) and (2.2) were obtained after some transformations from the local buckling critical stress relation of the long orthotropic uniformly compressed plate, presented in detail in Volmir (1968). For the special case of isotropic plates, there is $\gamma = 1 - \nu^2$.

- For multi-cell orthotropic columns (with n cells), analogously to formulas (2.1), we obtain the buckling stress from

$$\sigma_{crnh}^{loc} = k\frac{\pi^2 E_1}{12\gamma}\Big(\frac{t_{nh}}{b_{nh}}\Big)^2 = n^2 k\frac{\pi^2 E_1}{12\gamma}\Big(\frac{t_{nh}}{b_{1h}}\Big)^2$$
$$\sigma_{crnv}^{loc} = k\frac{\pi^2 E_1}{12\gamma}\Big(\frac{t_{nv}}{b_{nv}}\Big)^2 = n^2 k\frac{\pi^2 E_1}{12\gamma}\Big(\frac{t_{nv}}{b_{1v}}\Big)^2 \tag{2.3}$$

From the set *a priori* assumption on the same cross-section area of the single-cell and multi-cell column there result simple relations

$$t_{nv} = \frac{n}{3(n-1)}t_{1v} \qquad t_{nh} = \frac{n}{3(n-1)}t_{1h} \tag{2.4}$$

Comparing formulas (2.1) and (2.3) and remembering relations (2.4), for the considered multi-cell columns, the critical local buckling stress can be calculated from the approximate formula

$$\sigma_{crn}^{loc} = \alpha_n \sigma_{cr1}^{loc} \tag{2.5}$$

where obviously

$$\alpha_n = \frac{n^4}{9(n-1)^2} \qquad n = 2, 3, 4, \ldots \tag{2.6}$$

Relation (2.6) is valid for columns of rectangular and square cross-sections made of iso- and orthotropic materials. We note that increase of the parameter n (number of cells adjacent to one wall) causes an increase in the ratio t_n/b_n. According to formulas (2.1), (2.3) and (2.5), it is connected with a greater value of local buckling stress, so the coefficient α_n shows how many times the critical local buckling stress of the multi-cell column with n cells is greater than the critical buckling stress of the single cell column made of the same material and with the same cross-section area. The relation α_n as a function of the parameter n for rectangular cross-section columns is presented on a graph in Fig. 2. For $n = 1$, the coefficient $\alpha_n = 1$.

In Królak *et al.* (2007), formulas and graphs for different profiles for thin-walled multi-cell columns are given. Some of them – not only with rectangular cells – are presented in Fig. 3.

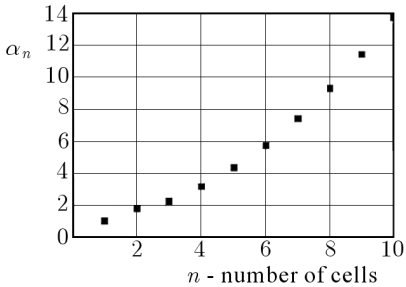

Fig. 2. Values of the coefficient α_n as a function of the number of cells n

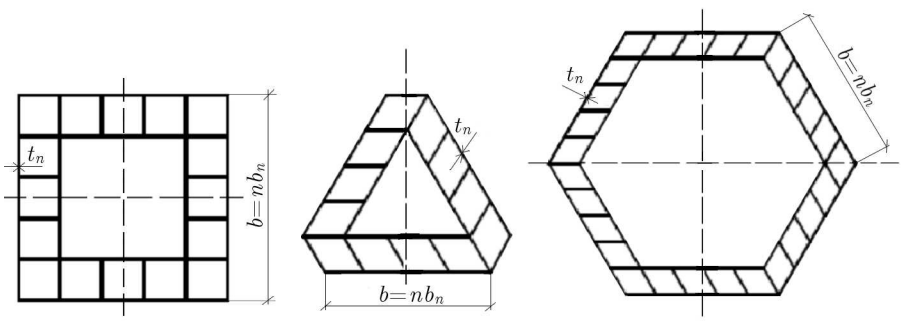

Fig. 3. Cross-sections of analysed columns

In Fig. 4, for different cross-sections of multi-cell columns graphs of the coefficient α_n as a function of the parameter n are presented.

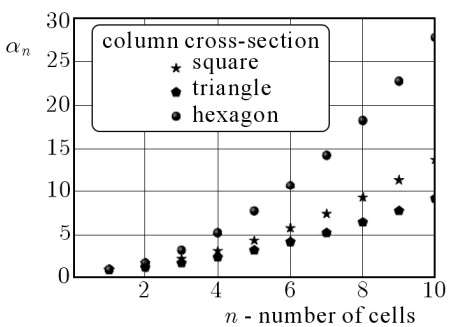

Fig. 4. Coefficient α_n as a function of the number of cells

3. Global buckling of multi-cell columns subjected to axial compression

The global buckling stress for a compressed multi-cell column simply supported at both ends is defined by Euler's formula

$$\sigma_{crn}^{gl} = \frac{\pi^2 (D_n)_{min}}{AL^2} \tag{3.1}$$

where $(D_n)_{min}$ is the minimal flexural stiffness of the column with the n-cell parameter, A – cross-section area, and L – column length. The cross-section areas of single-cell and multi-cell columns are equal, and so $A = 2(b_{1h}t_{1h} + b_{1v}t_{1v})$. For the multi-cell column, the formula of global buckling stress can be written as

$$\sigma_{crn}^{gl} = \beta_n \sigma_{cr1}^{gl} \tag{3.2}$$

where $\beta_n = (D_n)_{min}/(D_1)_{min}$. The variation of coefficient β_n as a function of the parameter n (number of cells) is plotted in Fig. 5.

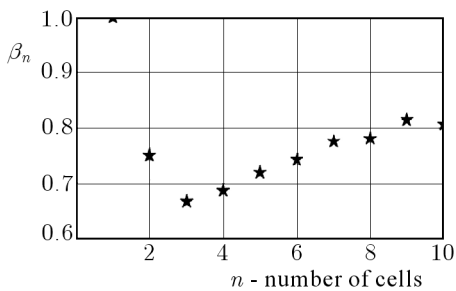

Fig. 5. Variation of the coefficient β_n as a function of the number of cells

It turns out from Figure 5 that the maximal decrease of the global buckling critical stress occurs for $n = 3$ (it is circa 33% of the critical stress of the single-cell column). For $n > 3$, the stress σ_{crn}^{gl} rises gradually with the growth of the parameter n and reaches nearly $0.8\sigma_{cr1}^{gl}$ for $n = 9$.

4. Experimental test on analysed columns

4.1. Description of tested thin-walled columns

The experimental tests of segments of columns were carried out on six models with rectangular and square cross-sections, that is:

- one model of a thin-walled column with single-cell square cross-section,
- three models of thin-walled multi-cell columns with square cross-sections and square cells,
- two models of thin-walled multi-cell columns with rectangular cross-sections.

The model of the single-cell column (marked as model 1) was made of a steel sheet of $t_1 = 1.24\,\text{mm}$ thickness. The cross-section of this model and its dimensions are presented in Fig. 6.

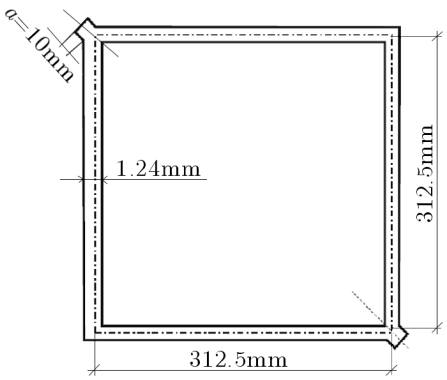

Fig. 6. Cross-section of model 1 and its dimensions

The presented model was made of two parts of correctly bent sheets connected in two corners by spot welding. The sticking out of the model outline welded elements were cut perpendicular to the model height not to carry the compressive load. The total height of the tested model (the length of the column segment between nodal lines of local buckling of its walls) was equal to the wall width ($L = b_1$). The material constants for the steel sheet were obtained from a tensile test and were as follows: $E = 2.0 \cdot 10^5\,\text{MPa}$, $\nu = 0.3$, $R_{0.2} = 179\,\text{MPa}$, $R_m = 313\,\text{MPa}$. The cross-section area of the model was $A = 4b_1t_1 = 4 \cdot 312.5 \cdot 1.24 = 1550\,\text{mm}^2$. The ratio of the wall width-to-thickness was $b_1/t_1 = 252$.

Three models of square multi-cell columns (models number 2, 3, 4) were made of a steel sheet of $t_1 = 0.5\,\text{mm}$ thickness. Five square cells were adjacent ($n = 5$) to the external wall. The cross-section of such a model is presented in Fig. 7.

The elements of these models were joined by spot welding. The internal walls of cells (between external and internal walls of the column) were made as a 'I-shape' profiles. They were cut of a steel sheet by laser technology and their 'flanges' were bent in the way shown in Fig. 8.

Fig. 7. Square cross-section of the multi-cell model

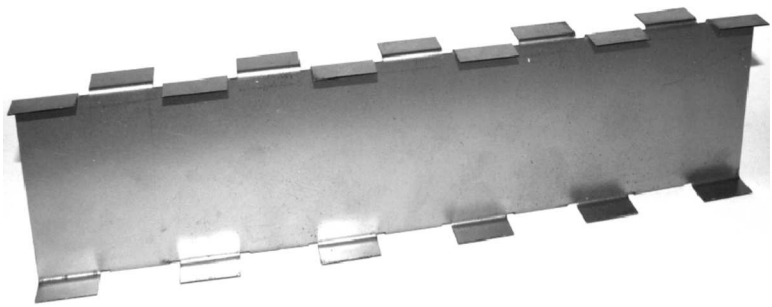

Fig. 8. Internal wall of the multi-cell model

The dimensions of the manufactured models slightly differ from each other because of what occurred during sheet bending and spot welding processes.

Table 1. Model dimensions

Model number	b [mm]	b_5 [mm]	t_5 [mm]	h [mm]	A [mm^2]
2	318	63.6	0.5	318	1526
3	322	64.4	0.5	322	1546
4	316	63.2	0.5	316	1517

The cross-section areas of all models – single- and multi-cell of square shapes were nearly equal to 1500 mm^2. The material properties of the steel sheet of thickness 0.5 mm, which was used for manufacturing of multi-cell models were as follows: $E = 1.97 \cdot 10^5$ MPa, $\nu = 0.3$, $\sigma_H = 140$ MPa,

$R_{0.2} = 202\,\text{MPa}$, $R_m = 315\,\text{MPa}$. In Fig. 9, there is a photography of one of the square multi-cell models. There were significant imperfections in tested models, especially in one of them made as a trial one. These were imperfections of model walls and differences of cell dimensions.

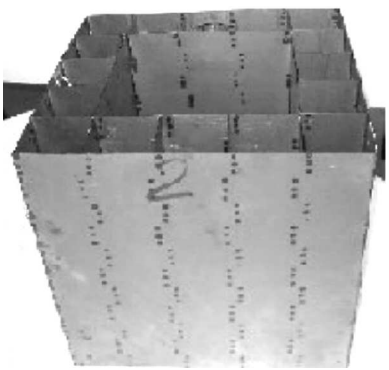

Fig. 9. Model of a square multi-cell column

Two models of thin-walled multi-cell columns with a rectangular shape and with rectangular cells (model 5 and 6) were made of brass sheets of $t_{5h} = 0.3\,\text{mm}$ and $t_{5v} = 0.6\,\text{mm}$ thicknesses. Number of cells (parameter $n = 5$) was equal for both models. The walls were joined by the break-head rivets with the diameter 2.2 mm. The rivets were used because it was impossible to connect the brass sheets by spot welding. The cross-sections of brass models and their dimensions are shown in Fig. 10.

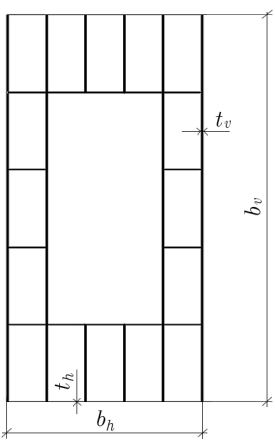

Fig. 10. Cross-section of the brass multi-cell column

The models differ between themselves with the rivets spacing and their layout. Figure 11 presents a photograph of the manufactured brass model.

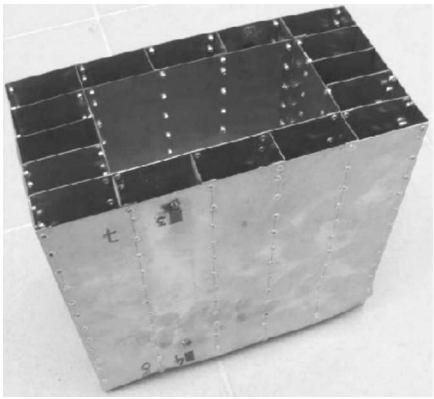

Fig. 11. Multi-cell model made of brass sheets

The material properties of brass sheets were as follows: $E = 1.0 \cdot 10^5$ MPa, $\nu = 0.3$, $\sigma_H = 100$ MPa, $R_{0.2} = 180$ MPa, $R_m = 256$ MPa.

4.2. Test stand description

A special test stand presented in Fig. 12 was designed and manufactured to perform experimental investigation of the multi-cell models.

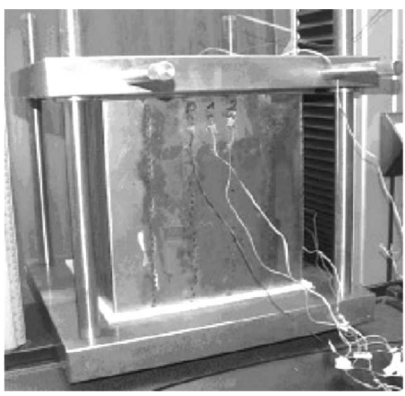

Fig. 12. Experimental stand

The upper movable plate of the stand can slide along four vertical bars which are fixed to the lower plate. Both plates are made of steel of thickness 45 mm. The high thickness of the plates provides small strains during

compression of the column, and the guide bars provide the mutually parallel position of the plates. As a result, a uniform shortening of all walls is achieved (symmetry of column). Between all loaded edges of the model and both – upper and lower steel plates, soft aluminum and foamed PCV plates are additionally placed to provide uniformly distributed compressive stresses in the pre-buckling state. Thickness of these plates is 5 and 3 mm for aluminum and PCV, respectively. Moreover, the PCV plates approximate the simply support conditions on loaded edges and remove pointwise contact between the edges and loading plates as well as possible stress concentration. In Fig. 13, dimples pressed in the PCV plate during model compression are shown.

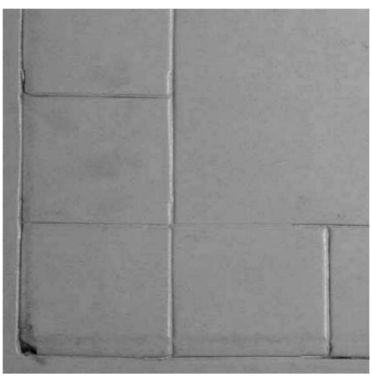

Fig. 13. Dimples in a foamed PCV plate

4.3. Conditions of experimental tests

The experimental tests were carried out on the multipurpose material testing machine INSTRON controlled by a PC unit. The applied equipment and software ensured automatic measurement of the loading force and the displacement of the upper plate of the test stand fixed in the testing machine. The walls of the tested model were bonded with strain-gages connected to the multi-channel bridge SPIDER (HBM), also controlled by PC. The deflections of selected points of external walls were measured by dial gauges with a low axial force of the plunger. The deflections were evaluated in points where the buckling wave summits were expected. The column in the testing machine and the testing system are presented in Fig. 14.

4.4. The aim of the experiments

The purpose of the experimental test was the analysis of behaviour of thin-walled multi-cell columns in following ranges: pre-buckling, buckling, post-

Fig. 14. The test stand and measuring equipment

buckling elastic, elastic-plastic and failure. The critical load of global buckling and ultimate load were the main values which were to be measured. The other parameters which influence the behaviour of columns, especially imperfections, were also observed.

The experimental tests were to prove:

- much higher resistance of multi-cell columns to local buckling than single-cell ones (with equal cross-section area),
- higher load carrying capacity of multi-cell columns than single-cell ones (better exploitation of material properties in multi-cell columns),
- correctness of derived formulas for local buckling stress of multi-cell columns.

The above problems are referenced in the following sections.

4.5. Results of experimental tests

4.5.1. Square cell models

The square shape cross-sections of column models (or segments of columns) were presented in Figs. 6 and 7, while their dimensions are drawn up in Table 1. The load shortening curves (L-S curves) of these models obtained from the INSTRON testing machine are compiled in Fig. 15. These are plots of the compressive force (without taking into account the upper pressing plate weight, which was nearly 1 kN) as a function of the upper plate displacement. This displacement depends on shortening of models height and dimples pressed

in the aluminum and foamed PCV plates. The aluminum plates were placed between edges and upper and lower steel pressing plates for models 1, 2, 3, 4, when for the last two models the PCV plates were added.

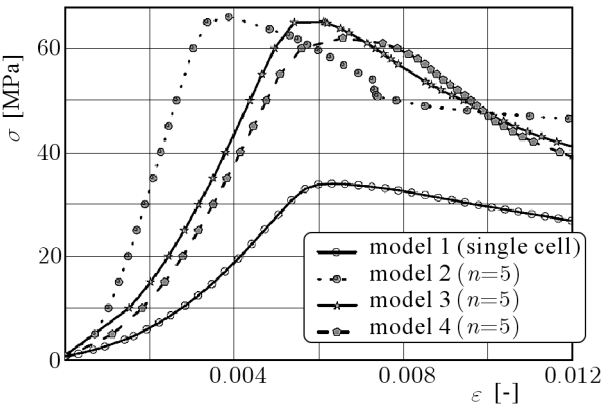

Fig. 15. L-S curves for square multi-cell columns

The results of tests are compared in Table 2.

Table 2. Results of experiments

Model number	A [mm^2]	σ_{cr}^{com} [MPa]	P_{cr}^{com} [kN]	P_{ult}^{exp} [kN]	σ_{ult}^{exp} [MPa]
1	1550	11.00	12.6	51.6	33.3
2	1526	44.69	68.2	101.6	66.6
3	1546	43.58	67.4	99.43	64.3
4	1517	45.26	68.6	94.64	62.4

The values of ultimate loads P_{ult}^{exp} (maximum value of the force in the L-S plot without weight of the upper pressing plate considered) were obtained directly from the experiment. The average ultimate stresses were determined from division of the ultimate force by model cross-section area. The average ultimate stress is ca 5.2 times smaller than the yield limit of the material used for model construction. It means that for a single-cell thin-walled column the strength of the material is exploited only in small amount. The obtained in the experiments the ultimate loads for three models of multi-cell columns (models 2, 3, 4) differ from themselves by 7.1% at most, while the average ultimate stresses σ_{ult}^{exp} by circa 6.5%. These stresses are 3.13 times less than the yield limit of the material used for model manufacturing, which means that the material of multi-cell column is exploited better. The usage of material properties in the single-cell column reached 19.25, while in the multi-cell model

ca 31.9%. The hundred percent usage of the material properties corresponds to full plasticity of cross-section area.

The critical force for local buckling of the single-cell column was determined both from the LSC of the column for loads in the range 0-50 kN (Fig. 16), and from the deflection plot of one wall center point as a function of load (Fig. 17).

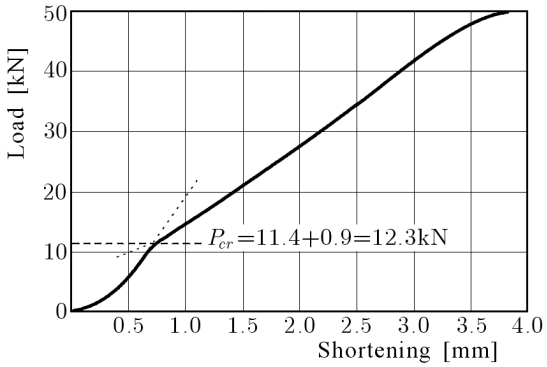

Fig. 16. Method of buckling load evaluation based on L-S curve

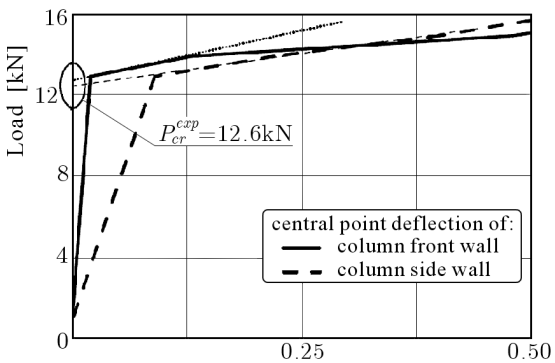

Fig. 17. Method of buckling load evaluation based on deflection plot

As shown in Figs. 16 and 17, the critical values of buckling load obtained in experiments are in the range of $P_{cr}^{exp} = 12.3\text{-}12.6$ kN.

The value of local buckling stress determined in laboratory tests is in the range of $\sigma_{cr}^{exp} = 7.9\text{-}8.1$ MPa.

In the tested models of multi-cell columns, classical local buckling phenomena were not observed. On the obtained LS curves, there is no characteristic inflection point which refers to the critical load (to change the column compressive stiffness). Theoretically, the classical buckling should occur in columns

without imperfection with so chosen geometry of the walls and boundary conditions as to all walls would immediately lose stability. It appeared from the carried out experiments that the multi-cell column walls with different imperfections (geometric and in the load input) buckle gradually under uniform compression. Mainly due to non-uniformly distributed load (caused by the lack of ideal contact between the wall edges and the compressive plates) the more loaded walls buckled earlier. At the moment when the last walls buckled, those buckled earlier worked in the post-buckling range. When the critical stress was comparatively high, it could be even an elastic-plastic state. From the moment when almost all or even all walls buckled, the increments of column shortening stay higher for the same increments of compressive load (what is caused by greater and greater deflections of walls). For this reason, the authors suggest to determine the critical load of local buckling (stress or force) of uniformly compressed multi-cell columns as the maximum load value, over which for an equal increment of compression the wall deflections grow (or grow the shortening increments). The Load Shortening Curve of multi-cell columns can be divided into a few phases:

- the initial phase, the structure 'settles' in bearings,
- the pre-buckling phase, when the number of buckled walls rises gradually,
- the critical state – the maximal load value over the tangent to the linear (or almost linear) part of the L-S plot,
- the post-buckling elastic range,
- the post-buckling elastic-plastic range, up to load carrying capacity (maximal load),
- the collapse phase.

For such a definition of the critical load, the critical local buckling forces amount ca $P_{cr}^{exp} = 80\,\mathrm{kN}$ for the tested three models of square multi-cell columns. After a detailed analysis of all L-S plots of models 2, 3 and 4, the local buckling forces and stresses were determined as follows

$$P_{cr2}^{exp} = 79\,\mathrm{kN} \qquad \sigma_{cr2} = 51.8\,\mathrm{MPa}$$
$$P_{cr3}^{exp} = 81\,\mathrm{kN} \qquad \sigma_{cr3} = 52.0\,\mathrm{MPa}$$
$$P_{cr4}^{exp} = 80\,\mathrm{kN} \qquad \sigma_{cr4} = 52.7\,\mathrm{MPa}$$

4.5.2. Models of rectangular cross-section columns

The cross-section of two models of multi-cell columns with rectangular shapes are shown in Fig. 18, and their dimensions are given in Table 3.

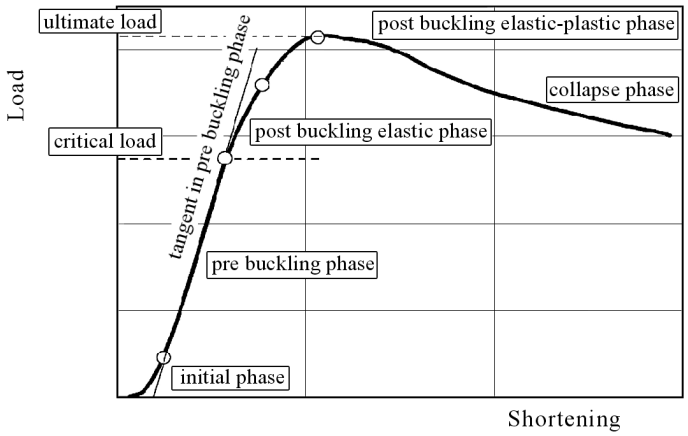

Fig. 18. Load Shortening Curve

Table 3. Rectangular cells dimensions

Model number	b_v [mm]	b_h [mm]	b_{v5} [mm]	t_{v5} [mm]	b_{h5} [mm]	t_{h5} [mm]	L [mm]	A [mm^2]
5, 6	250	125	50	0.6	25	0.3	250	900

These two models were made of brass sheets. The thickness and width of cell walls were selected to have the same thickness-to-width ratios

$$\frac{t_{5h}}{b_{5h}} = \frac{t_{5v}}{b_{5v}} = 1.2 \cdot 10^{-2}$$

The models differed from each other with the rivet spacing and layout. The L-S plots of these models are presented in Fig. 19. The results of experiments are compiled in Table 4.

Table 4. Results of experiments

Model number	σ_{cr}^{com} [MPa]	P_{cr}^{com} [kN]	P_{ult}^{exp} [kN]
5	52.06	46.85	50.70

The average ultimate stresses are approximately 3.32 times lower than the yield limit of used brass sheets material. Therefore, the material properties of brass were exploited in 30.2%. The critical loads for both rectangular multi-cell models were determined according to the definition given in 3.5.1 (Fig. 18). The critical stresses of both models are mutually close (they differ by 2% only).

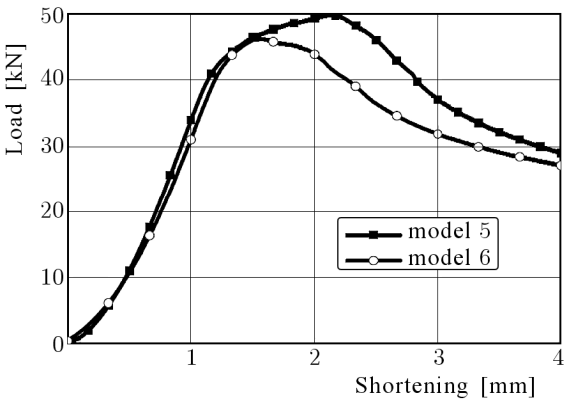

Fig. 19. L-S curve of rectangular multi-cell models

5. Results of numerical computations

For the compressed multi-cell column of a square or rhomboidal shape with equal width of all walls simply supported on loaded edges, the critical stress of local buckling can be approximated (calculated) from (2.3) or (2.4).

The buckling load factor k can be determined numerically from the analysis of one cell of the column (it is valid for cells of arbitrary cross-section shapes and wall thickness). The most accurate value of local buckling critical stress can be determined with FEM software considering the whole column.

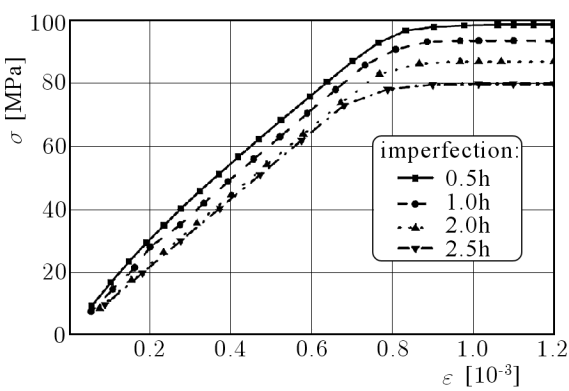

Fig. 20. Influence of initial imperfections

Assuming that a single wall of the square or rhomboidal multi-cell column is a long compressed plate with all edges simple supported, the load carrying capacity can be calculated as an average ultimate stress for the wall of equal to

the other walls thickness. In Fig. 20, it is shown that imperfection amplitudes have significant influence on the average ultimate stress.

The plots presented in Fig. 20 were obtained by an analytical-numerical method with the assumption that the material is linearly elastic and perfectly plastic and had following parameters: $E = 2{\cdot}10^5$ MPa, $\nu = 0.3$, $R_e = 203$ MPa. These are properties of a steel sheet of thickness equal to 0.5 mm, which was used to manufacture models of the square multi-cell columns.

The results of computations of ultimate loads performed with FEM packages are reliable only when the real tensile test data are implemented in the numerical calculations. A case of numerical computations carried out with the FEM package ANSYS is submitted in the next two figures.

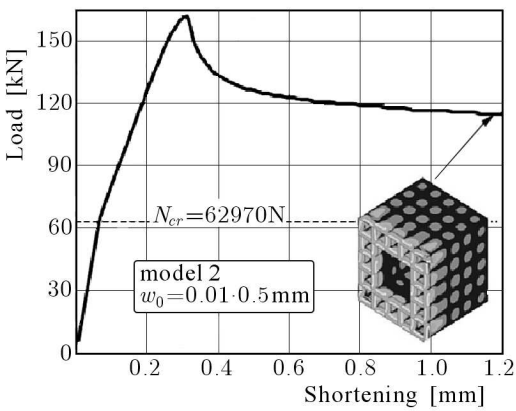

Fig. 21. L-S curve for the square multi-cell model obtained in FEA

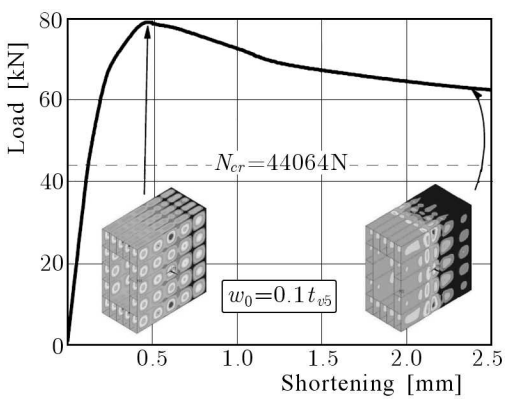

Fig. 22. L-S curve for the rectangular multi-cell model obtained in FEA

6. Comparison of experimental and numerical results

The results of local buckling stresses and ultimate loads obtained in experimental tests and in numerical computations are presented in Table 5.

7. Conclusions

From the carried out experimental tests, the following conclusions can be drawn:

- For compressed multi-cell columns of equal dimensions, equal cross-section areas, made of the same materials and exactly in the same way supported:
  - local buckling stress of walls increases with the increase of the parameter n – the number of cells adjacent to the single column external wall (which is not equivalent to the increase of the total number of column cells),
  - for some value of the parameter n, the whole column cross-section can plasticize before local buckling of it occurs,
  - for a multiple number of adjacent cells, the width of the single wall becomes small and local buckling of the whole wall can occur instead of the single-cell wall,
  - when the parameter n increases, the ultimate load of the column increases too, but this progress is much slower than that of the local buckling critical stress,
  - the classical local buckling phenomena did not occur for the tested models of multi-cell columns because of different types of imperfections,
  - with the progress of compression, the number of buckled cell walls rises,
  - a change of stiffness of the multi-cell column takes place in practice after all walls have buckled (some of them are in the elastic post buckling range or even elastic-plastic state),
  - the suggested method to determine the local buckling critical stress based on the experimental L-S curves seems to be justified for such structures,

Table 5

Model No.	Cross-section shape	Cell wall width [mm]	Wall thickness [mm]	Cross-section area [mm^2]	Ultimate load		Critical load		Average ultimate stress		Critical stress			Material
					Exp. [kN]	Comp. [kN]	Exp. [kN]	Comp. [kN]	Exp. [MPa]	Comp. [MPa]	Exp. [MPa]	Comp. [MPa]	Introd. form.	
1	Squ. $n = 1$	312.5	1.24	1550	51.6	66.0	12.6	17.1	33.3	42.6	8.1	11.0	11.4	steel
2	Squ. $n = 5$	63.6	0.5	1526	101.6	156.2	67.0	63.0	66.6	102.3	43.9	41.3	44.7	steel
3	Squ. $n = 5$	64.4	0.5	1546	99.4	157.0	68.0	62.2	64.3	101.6	44.0	40.2	43.6	steel
4	Squ. $n = 5$	63.2	0.5	1517	94.6	155.2	62.0	63.4	62.4	102.3	40.9	41.1	45.3	steel
5	Rectangle $n = 5$	$b_v = 50$ $b_h = 25$	$t_v = 0.6$ $t_h = 0.3$	900	50.7	79.0	39.5	44.1	56.3	87.8	43.9	49.0	52.0	brass
6	Rectangle $n = 5$	$b_v = 50$ $b_h = 25$	$t_v = 0.6$ $t_h = 0.3$	900	47.2	79.0	40.2	44.1	52.4	87.8	44.7	49.0	52.0	brass

  - great diversity of geometrical imperfections of multiple column walls causes that their influence on decreasing the ultimate load is less significant than for the single-cell column,
  - the global buckling stress of the multi-cell column decreases in the case when the parameter n equals 2 or 3 and increases with n, approaching gradually the critical stress of the single-cell column,

- For a greater number of cells, the interaction of different modes of buckling may take place, which is difficult to predict in theoretical considerations and which was proved in the numerical analysis.

The experimental tests gave quite good agreement of the results for compatible models and between the experimental and numerical data, which is often difficult to achieve in stability investigations.

Acknowledgemment

The current work has been done in the frame of the research project KBN 4T07A02829.

References

1. Chen W., Wierzbicki T., 2001, Relative ments of single cell, multi-cell and foam-filled thin-walled structures in energy absorption, *Thin-Walled Structures*, **39**, 287-306
2. Grądzki R., Kowal-Michalska K., 1985, Elastic and elasto-platic buckling of thin-walled columns subjected to uniform compression, *Thin-Walled Structures Journal*, **3**, 93-108
3. Kim H.S., 2002, New extruded multi-cell aluminum profile for maximum crash energy and weight efficiency, *Thin-Walled Structures*, **40**, 311-328
4. Kołakowski Z., Kowal-Michalska K., 1999, *Selected Problems of Instability in Composite Structures*, Technical University of Lodz, Łódź, Poland
5. Królak M., Kowal-Michalska K., 2004a, Stability and load-carrying capacity of multi-cell columns subjected to compression, *Proc. of IV Coupled Instabilities in Metal Structures, CIMS 2004*, Pignatario M. (Edit.), Rome, 213-222
6. Królak M., Kowal-Michalska K., 2004b, Stability and ultimate load of multi-cell orthotropic columns subjected to compression, *Proc. of the 8-th SSTA Conference*, Jurata, Poland, 235-239

7. KRÓLAK M., KOWAL-MICHALSKA K., MANIA R., ŚWINIARSKI J., 2006, Badania doświadczalne stateczności i nośności modeli cienkościennych słupów wielokomorowych poddanych równomiernemu ściskaniu, *Materiały XXII Sympozjum Mechaniki Eksperymentalnej Ciała Stałego*, Jachranka, 297-302

8. KRÓLAK M., KOWAL-MICHALSKA K., ŚWINIARSKI J., 2007, Stateczność i nośnośc cienkościennych słupów wielokomorowych równomiernie ściskanych, *Materiały XX Konferencji Problemy Rozwoju Maszyn Roboczych*, Zakopane

9. MAQUOI R., MASSONET CH., 1971, Nonlinear theory of post-buckling resistance of large stiffened box girders, *IABSE Publications*, **31**, 11, 91-140

10. MASSONET CH., MAQUOI R., 1973, New theory and tests on the ultimate strength of stiffened box girders, *Proc. Int. Confer. on Steel Box Girders Bridges*, The Inst. of Civil Engrs, Loudres

11. VOLMIR S.A., 1968, *Stability of Deforming Systems*, Science Moscow [in Russian]

Stateczność i nośność wielokomorowych cienkościennych słupów o prostokątnych przekrojach poprzecznych

Streszczenie

Praca poświęcona jest teoretycznej, numerycznej i doświadczalnej analizie stateczności i nośności granicznej wielokomorowych cienkościennych słupów o prostokątnych i kwadratowych przekrojach poprzecznych poddanych osiowemu ściskaniu (odpowiadającemu równomiernemu skróceniu słupa). Rozważania teoretyczne dotyczą lokalnej i globalnej utraty stateczności wielokomorowych ortotropowych słupów o obrysie prostokątnym, z prostokątnymi komorami. Wykazano, że dla wielokomorowego słupa wykonanego z tego samego materiału i o takim samym polu przekroju poprzecznego wartości lokalnego naprężenia krytycznego ścian słupa wzrastają gwałtownie wraz ze wzrostem liczby komór. Doświadczenia przeprowadzone dla izotropowych słupów potwierdziły wzrost zarówno naprężeń krytycznych, jak i nośności badanych modeli wraz ze wzrostem komór. W pracy podano pewne wnioski, które mogą być przydatne przy projektowaniu cienkościennych słupów o przekrojach skrzynkowych.

Manuscript received July 23, 2008; accepted for print November 18, 2008